Letter

Interband scattering- and nematicity-induced quantum oscillation frequency in FeSe

Valentin Leeb [1,2] and Johannes Knolle [1,2,3]

[1] *Technical University of Munich, TUM School of Natural Sciences, Physics Department, TQM, 85748 Garching, Germany*

[2] *Munich Center for Quantum Science and Technology (MCQST), Schellingstr. 4, 80799 München, Germany*

[3] *Blackett Laboratory, Imperial College London, London SW7 2AZ, United Kingdom*

(Received 8 September 2023; revised 4 November 2023; accepted 25 January 2024; published 20 February 2024)

Understanding the nematic phase observed in the iron-chalcogenide materials is crucial for describing their superconducting pairing. Experiments on $FeSe_{1-x}S_x$ showed that one of the slow Shubnikov-de Haas quantum oscillation frequencies disappears when tuning the material out of the nematic phase via chemical substitution or pressure, which has been interpreted as a Lifshitz transition [Coldea *et al.*, npj Quantum Mater. **4**, 2 (2019); Reiss *et al.*, Nat. Phys. **16**, 89 (2020)]. Here, we present a generic, alternative scenario for a nematicity-induced sharp quantum oscillation frequency, which disappears in the tetragonal phase and is not connected to an underlying Fermi surface pocket. We show that different microscopic interband scattering mechanisms—for example, orbital-selective scattering—in conjunction with nematic order can give rise to this quantum oscillation frequency beyond the standard Onsager relation. We discuss implications for iron-chalcogenides and the interpretation of quantum oscillations in other correlated materials.

DOI: 10.1103/PhysRevB.109.L081109

Introduction. The availability of experimental methods, which are able to correctly identify the low-energy electronic structure of quantum materials, is critical for understanding their emergent phenomena such as superconductivity, various density, waves, or nematic orders. For example, angle-resolved photoemission spectroscopy (ARPES) on the cuprate materials confirmed that a single-band Hubbard-like description is a reasonable starting point for modeling their low-energy structure [1], but iron-based superconductors require a multiband, multiorbital description [2–4]. Beyond ARPES, quantum oscillation (QO) measurements are an exceptionally sensitive tool for measuring Fermi surface (FS) geometries as well as interaction effects via extracting the effective masses from the temperature dependence [5]. For example, QO studies famously confirmed the presence of a closed FS pocket in underdoped cuprates in a field [6,7] or observed the emergence of small pockets in the spin density wave parent phase of iron-based superconducting compounds [8–10].

The interpretation of QOs, as measured in transport or thermodynamic observables, is based on the famous Onsager relation, which ascribes each QO frequency to a semiclassical FS orbit [5,13]. In the past years, this canonical description has been challenged by the observation of anomalous QOs in correlated insulators [14,15], which motivated a number of works revisiting the basic theory of QOs [16–28]. Very recently, forbidden QO frequencies have been reported in the multifold semimetal CoSi [29], which generalize so-called magneto-inter-sub-band oscillations known in coupled two-dimensional (2D) electron gases [30–32] to generic bulk metals [33]. In Ref. [29] it was proposed that QO of the quasiparticle lifetime in systems with multiple allowed FS orbits can lead to new combination frequencies without a corresponding semiclassical FS trajectory.

Here, we propose an alternative explanation for the QO spectra measured in the iron-chalcogenide superconductor $FeSe_{1-x}S_x$, which leads to an alternative identification of its low-energy electronic structure with direct implications for the superconducting pairing. Iron chalcogenides are unique among the iron-based superconductors as they show an orthorhombic distortion without stripe magnetism, i.e., pristine FeSe is already in a nematic phase [34–36]. Recently it was reported that one of the observed slow QO frequencies (labeled as λ in the experimental data) vanishes when tuning out of the nematic into the tetragonal phase, via pressure in $FeSe_{0.89}S_{0.11}$ [12] or via isoelectronic substitution in $FeSe_{1-x}S_x$ [11]. Following Onsager's standard theory it has been interpreted as a Lifshitz transition, i.e., a FS pocket only present in the nematic phase and disappears at the nematic quantum critical point [12]. As an alternative scenario, we show here that an additional slow QO frequency without an underlying FS orbit can naturally appear in an electronic nematic phase.

Our scenario requires the following features of iron chalcogenides [37–41]: (i) the FS consists of several pockets, in particular two electron pockets (labeled here as β_x and β_y) around the Y and X point of the Brillouin zone (BZ), see Fig. 1(b). β_x (β_y) has almost pure $d_{xz}(d_{yz})$ orbital character with some d_{xy} content. They are related to each other via a C_4 rotation in the tetragonal phase. (ii) When tuning into nematic phase with broken rotational symmetry (reduced to C_2) one of the pockets spontaneously increases in size, whereas the other one shrinks, see Fig. 1(a). In the QO spectrum, this is visible by the split up of one formerly degenerate QO frequency into two frequencies. (iii) A strong interpocket scattering between the β_x and β_y pocket exists [34,42–44]. It can be caused either by orbital selective impurity scattering over the d_{xy}-channel, low-momentum scattering, collective fluctuations or, most likely, a combination of all. As a result, we will show

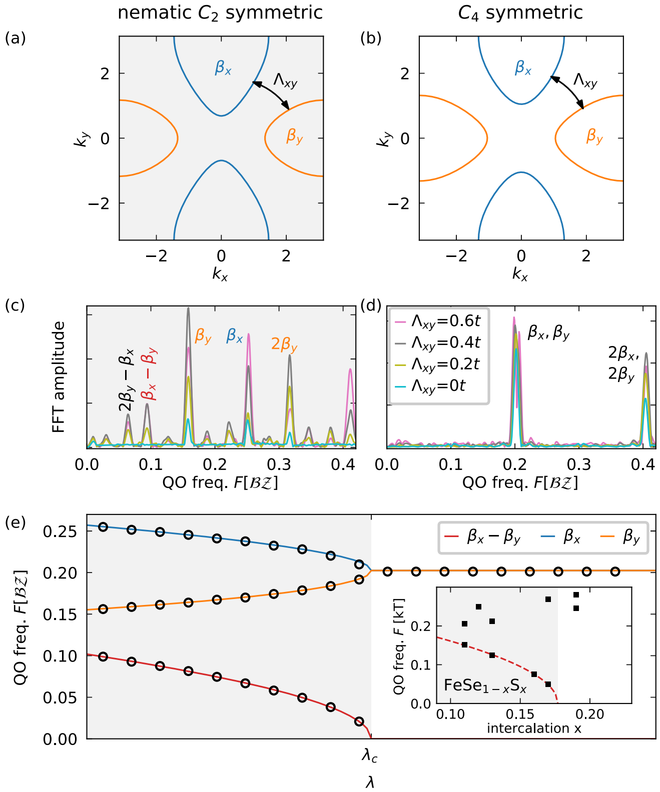

FIG. 1. (b) FS of a minimal model including only two electron pockets β_x, β_y with different orbital character. (a) In the nematic phase the β_x pocket spontaneously grows whereas β_y shrinks, see (c) and (d) for representative numerical SdH QO spectra for the different phases. (e) In the nematic phase (gray background) the degenerate frequency of the C_4 symmetric phase splits up into two frequencies (blue, orange), each associated with one FS. When taking interband coupling from impurities (Λ_{xy}), see (a), (b), into account a third frequency (red), which is exactly the difference of the basis frequencies $\beta_x - \beta_y$ appears in the nematic phase. We fixed $t_1/2 = t_2 = t$, $\mu = -3t$. The inset of (e) shows the experimentally detected peak frequencies in $FeSe_{1-x}S_x$ [11]. The red dashed line ($\propto \sqrt{\lambda_c - \lambda}$) is a guide to the eye highlighting the emergent frequency in the nematic phase, identified as λ in Refs. [11,12].

that a new slow QO frequency, set by the difference of the β_x and β_y frequencies, emerges.

We argue that our theory can not only explain the slow SdH QO frequency observed in iron chalcogenides, but also discuss that it provides further support for the robustness of $s_\pm$ superconducting pairing. We note that we do not aim towards a full quantitative description of the complicated QO spectrum of FeSe but rather focus on presenting a theory for the additional slow QO frequency appearing in the nematic phase, thus, concentrating on model descriptions with the minimal ingredients of the electronic structure (e.g., neglecting aspects of three dimensionality).

The Letter is organized as follows. We first introduce a basic two-band model, which captures the minimal features of an electronic nematic phase transition. We then show that interpocket scattering leads to a new QO frequency in a full lattice calculation of the SdH effect, including the orbital magnetic field via Peierls substitution. Next, we discuss a more microscopic multiorbital description of iron chalcogenides and identify different scattering mechanisms leading to strong interelectron pocket coupling. Again, we confirm the emergence of a slow nematicity-induced frequency in a full lattice calculation. We close with a summary and outlook.

Minimal two-pocket model. First, we consider a minimal model with two electron pockets and the Hamiltonian

$$H_0 = \sum_{\boldsymbol{k}} (\epsilon_{x,\boldsymbol{k}} - \delta\mu) d^\dagger_{x,\boldsymbol{k}} d_{x,\boldsymbol{k}} + (\epsilon_{y,\boldsymbol{k}} + \delta\mu) d^\dagger_{y,\boldsymbol{k}} d_{y,\boldsymbol{k}} \quad (1)$$

with the dispersion $\epsilon_{x,\boldsymbol{k}} = -2t_1 \cos k_x + 2t_2 \cos k_y$ and $\epsilon_{y,\boldsymbol{k}} = 2t_2 \cos k_x - 2t_1 \cos k_y$. It consists of a β_x-FS pocket around the Y point and a β_y-Fermi pocket around the X point, see Fig. 1(b). For $\delta\mu = 0$ the Hamiltonian is invariant under the C_4 rotation $(k_x, k_y) \to (k_y, -k_x)$, $(d_x, d_y) \to (d_y, -d_x)$. Additional density-density interactions $\sum_{\boldsymbol{r},\alpha,\beta} d^\dagger_{\alpha,\boldsymbol{r}} d_{\alpha,\boldsymbol{r}} d^\dagger_{\beta,\boldsymbol{r}} d_{\beta,\boldsymbol{r}}$ can induce a nematic transition with a finite orbital asymmetry $\delta\mu \neq 0$ breaking the C_4 rotation symmetry. Mean-field calculations confirm that $\delta\mu$ becomes nonzero for interactions above a critical threshold [45]. Thus, $\delta\mu$ serves as an order parameter for a nematic phase transition, which is manifest in the band structure by the spontaneous growth/shrinking of the two inequivalent pockets, see Fig. 1(a). We note that additional FS pockets are present in FeSe and change properties of the nematic phase quantitatively but are not relevant for our purpose.

In practice an external parameter λ tunes the effective interaction strength, e.g., via a change of applied pressure [12] or chemical substitution [11]. Again, the precise relation between $\delta\mu(\lambda)$ and λ depends on microscopic details but we assume in the following the generic form of a second-order phase transition $\delta\mu \propto (\lambda_c - \lambda)^\alpha \theta(\lambda_c - \lambda)$ and fix, for simplicity, the exponent to be of the standard mean-field behavior $\alpha = 1/2$.

Following our recent works [29,33], we introduce a scattering contribution between the two electron pockets via impurities

$$H_{\text{imp}} = \sum_{\boldsymbol{r}} \Lambda_{xy,\boldsymbol{r}} d^\dagger_{x,\boldsymbol{r}} d_{y,\boldsymbol{r}} + \text{H.c.}, \quad (2)$$

where $\Lambda_{xy,\boldsymbol{r}}$ are drawn randomly, independently, and uniformly in space from the interval $[-\Lambda_{xy}/2, \Lambda_{xy}/2]$. On average the system retains its translation and rotation symmetry. For simplicity we set the intraorbital part of the impurities, i.e., Λ_{xx} and Λ_{yy} to zero, as they will only suppress the amplitude of all QO frequencies [33].

We include a magnetic field by standard Peierls substitution, effectively inserting a flux Φ in each plaquette of the square lattice. We have implemented the hopping Hamiltonian with magnetic field and impurities for system sizes up to 300×300 lattice sites. We determined the conductance through the Landau-Büttiker algorithm using the PYTHON package KWANT [46] and observed SdH oscillations of the conductance as function of $1/\Phi$. We then analyzed the Fourier transformation in $2\pi/\Phi$ with standard QO techniques, which include subtraction of a polynomial background, zero padding, and windowing, see Supplemental Material (SM) [47] (see also Refs. [5,46,48,49] therein). Representative Fourier spectra for the tetragonal (C_4 symmetric)

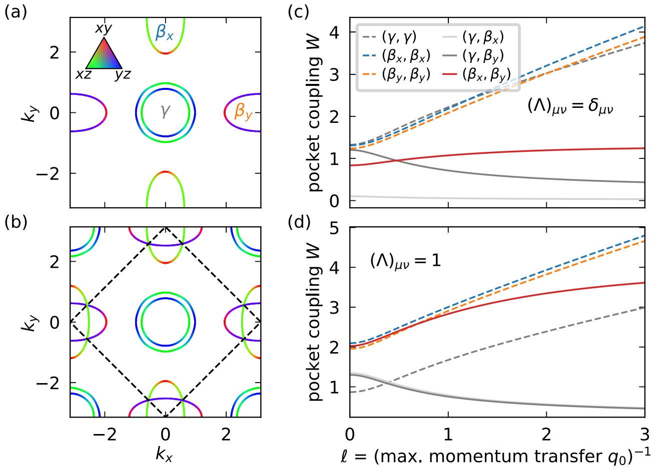

FIG. 2. (a) Typical FS of the three-orbital model in the nematic phase. Colors indicate the orbital character. (b) Buckling enlarges the unit cell, which leads to a back-folded FS in the reduced Brillouin zone (black dashed). (c) FS integrated inter- and intrapocket scattering strength for $(\Lambda)_{\mu\nu} = \delta_{\mu\nu}$ showing that the coupling W_{β_x,β_y} is dominant. It increases for small momentum scattering, i.e., $1/q_0 \to \infty$. Any other type of interorbit scattering enlarges the coupling of β_x and β_y even further, see (d) where $(\Lambda)_{\mu\nu} = 1$.

and nematic phase are shown in Figs. 1(c) and 1(d), where the frequencies are shown in units of the area of the BZ.

The Fourier spectrum of the SdH oscillations features, as expected from Onsager's relation, peaks at frequencies $F_\beta = S_\beta/2\pi e$, which correspond to the area of the respective FSs S_β and higher harmonics thereof. As our main finding, the spectrum has clear peaks at combination frequencies in the nematic phase, most dominantly $\beta_x - \beta_y$. Crucially, this frequency does not have an underlying FS or semiclassical orbit of any kind but is a consequence of QO of the quasiparticle lifetime. We note that this is in accordance with our recent analytical work [33], which we confirm here in a numerical lattice calculation. Additionally, we observe a weak main peak splitting of degenerate frequencies for sizable impurity scattering $\Lambda_{xy} \gtrsim 0.4t$, see Fig. 1(d), whose origin is unclear and does not appear in perturbative analytical calculations [33].

In Fig. 1(e), we plot the frequencies of the three strongest signals for weak interorbit scattering as a function of the external parameter λ tuning through the nematic transition. When increasing the nematic order, the main frequency peak splits into two, and the additional low-frequency $\beta_x - \beta_y$ oscillation emerges similar to the experimental data, see inset.

Multiorbital model. After studying a minimal two-band model, we next want to understand the possible origin of a strong interpocket scattering. Therefore, we need to take the multiorbital character of iron chalcogenides into account. In order to keep the numerical lattice calculations tractable we focus on the following key features, see Fig. 2(a): (i) two electronlike elliptical pockets β_x and β_y around the Y and X points, which have mainly d_{xz} and d_{yz} orbital character but in addition also an admixture of d_{xy} orbitals; (ii) one (or depending on the precise model and parameter regime also two) holelike circular pockets γ around the Γ point, which have mixed d_{xz} and d_{yz} orbital character; (iii) only the electron pockets β_x and β_y have additional d_{xy} orbital character.

All features (i)–(iii) are captured by a three-orbital model [45] with d_{xz}, d_{yz}, and d_{xy} orbitals (denoted by xz, yz, xy). Introducing $\boldsymbol{\Psi}_{\boldsymbol{k}} = (d_{\boldsymbol{k},xz}, d_{\boldsymbol{k},yz}, d_{\boldsymbol{k},xy})$, the Hamiltonian reads

$$H_0 = \sum_{\boldsymbol{k}} \boldsymbol{\Psi}_{\boldsymbol{k}}^\dagger (T[\boldsymbol{k}] - \mu)\boldsymbol{\Psi}_{\boldsymbol{k}} + \delta\mu \begin{pmatrix} d_{\boldsymbol{k},xz} \\ d_{\boldsymbol{k},yz} \end{pmatrix}^\dagger \sigma^z \begin{pmatrix} d_{\boldsymbol{k},xz} \\ d_{\boldsymbol{k},yz} \end{pmatrix}, \quad (3)$$

where $T[\boldsymbol{k}]$ is a 3×3 matrix, which depends on the electronic hopping strengths between the orbitals. The real-space form of the Hamiltonian, $T[\boldsymbol{k}]$ and the parameters are given in the SM [47].

In the tetragonal phase, with $\delta\mu = 0$, the Hamiltonian is again invariant under the C_4 rotation $(k_x, k_y) \to (k_y, -k_x)$, $(d_x, d_y) \to (d_y, -d_x)$. Similar to the toy model from above, a nematic phase is characterized by a finite $\delta\mu$ where the rotation symmetry is reduced to a $\mathbb{Z}_2$ reflection symmetry/C_2 rotation symmetry.

The parameter $\delta\mu$ is again an effective, emergent parameter but now we can relate its microscopic origin to orbital ordering. For example the interorbital density interaction between xz and yz orbitals

$$H_{\text{int}} = U \sum_{\boldsymbol{r}} d_{\boldsymbol{r},xz}^\dagger d_{\boldsymbol{r},xz} d_{\boldsymbol{r},yz}^\dagger d_{\boldsymbol{r},yz} \quad (4)$$

can be decoupled in mean field to obtain a self-consistent order parameter for the nematic (now orbital ordering) transition leading to $\delta\mu = U(\langle d_{\boldsymbol{r},xz}^\dagger d_{\boldsymbol{r},xz}\rangle - \langle d_{\boldsymbol{r},yz}^\dagger d_{\boldsymbol{r},yz}\rangle)/2$. A typical FS within the nematic phase is shown in Fig. 2(a).

We note that this role of orbital ordering, or an imbalance of the orbital occupation, in the nematic phase has been confirmed in a number of experiments [38,39] most recently via x-ray linear dichroism [40]. While our minimal three-orbital model captures the key features, the precise asymmetry of the γ hole pocket(s) in the nematic phase of FeSe is more complicated, however, its shape does not affect our new findings.

Impurities and orbital selective scattering. As confirmed in our two-band model numerically and expected from analytical calculations [33], a nematicity-induced difference frequency requires a sizable coupling of the pockets β_x and β_y. The absence of other frequency combinations points towards a negligible coupling of β_i and γ. We next investigate the origin of this coupling in terms of the d-orbital dependent scattering. Therefore, we consider impurities in the orbital basis

$$H_{\text{imp}} = \sum_{\boldsymbol{r}} \sum_{\boldsymbol{r}_i} V(\boldsymbol{r} - \boldsymbol{r}_i) \boldsymbol{\Psi}_{\boldsymbol{r}}^\dagger \Lambda_{\boldsymbol{r}_i} \boldsymbol{\Psi}_{\boldsymbol{r}} \quad (5)$$

with the scattering vertex $\Lambda_{\boldsymbol{r}_i}$ a random Hermitian matrix with mean 0 and variance Λ^2. Note, impurities respect the $\pi/2$-rotation symmetry only on average. Similarly, impurities located at $\boldsymbol{r}_i$ are distributed randomly and uniformly such that the systems remains on average translationally invariant. We model the interaction of electrons with impurities by a screened Coulomb interaction V_ℓ of Yukawa type with screening length ℓ [50].

We quantify the coupling $W_{\alpha,\alpha'}$ of FS orbits α and α' by integrating the scattering amplitudes of all possible processes between them

$$W_{\alpha,\alpha'} = \oint_{\boldsymbol{k}\in\alpha} \oint_{\boldsymbol{k}'\in\alpha'} \Bigg| \qquad \Bigg| \tag{6}$$

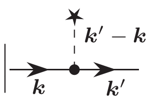

$$= \oint_{\boldsymbol{k}\in\alpha} \oint_{\boldsymbol{k}'\in\alpha'} |\tilde{V}_\ell(\boldsymbol{k}'-\boldsymbol{k})\mathcal{U}(\boldsymbol{k}')^\dagger \Lambda \mathcal{U}(\boldsymbol{k})|. \tag{7}$$

Here, $\mathcal{U}(\boldsymbol{k})$ is the transformation, which diagonalizes H_0 for a each momentum. The Fourier transform of the screened Coulomb interaction $\tilde{V}_\ell = \mathcal{N}_\ell/(\boldsymbol{k}^2 + 1/\ell^2)$ allows only scattering up to a maximal momentum $q_0 = 1/\ell$ ($\mathcal{N}_\ell$ is a normalization constant).

Iron chalcogenides have a two-site unit cell [37], which leads to a folding of the $T[\boldsymbol{k} + (\pi, \pi)]$ bands onto the $T[\boldsymbol{k}]$ bands. The FS in the reduced Brillouin zone is shown in Fig. 2(b), where now the pockets β_x and β_y lay on top of each other. This admits a large scattering between the β_x and β_y pockets because the screened Coulomb interaction favors low-momentum scattering. In Figs. 2(c) and 2(d) we show quantitatively that for diagonal or uniform scattering vertices Λ in the orbital components, the coupling W_{β_x,β_y} is the biggest interpocket coupling for a sizable screening length $\ell \gtrsim 0.5$ and of the same size as the intraorbit couplings.

There are several additional mechanisms, which increase W_{β_x,β_y} even further. Crucially, orbital-selective scattering, i.e., a dominating $\Lambda_{xy,xy}$ component of the vertex, leads to a large coupling of exclusively β_x and β_y pockets. Additionally, any off-diagonal element of Λ, i.e., xz/yz to xy and xz to yz scattering, strongly enhances the interpocket coupling W_{β_x,β_y}. Overall, there is generically a sizable coupling between the electron pockets.

An exclusive coupling of the electron pockets β_x, β_y can be modeled by orbital selective scattering over the $\Lambda_{xy,xy}$ channel. The analysis above suggests that this coupling is indeed dominating. For our numerical simulation of the SdH effect we, therefore, focus on short-ranged impurities $V(\boldsymbol{r}) \propto \delta(\boldsymbol{r})$ with an orbital selective scattering vertex $(\Lambda)_{ij} = \delta_{i3}\delta_{j3}\Lambda_{xy}$ with only the xy component $\Lambda_{xy,xy}$ being nonzero. We note that experiments indeed suggest that the xy-orbital part of the FS is heavy, leading to a large dominating density of d_{xy} states for scattering [37].

Slow QO frequency from orbital selective scattering. Finally, we evaluate the conductance in orbital magnetic fields through samples of sizes up to 400×400 sites with orbital selective impurities within the nematic phase. The dominant SdH peaks in the Fourier spectrum, see Fig. 3(a), are set by the FSs β_x, β_y, γ and higher harmonics thereof. The combination frequencies $\beta_x - \beta_y$ and $\beta_x + \beta_y$ are clearly visible and, additionally, a variety of subleading higher-order terms appear whose strength depends on the strength of the impurity scattering. In the bottom Fig. 3(b) we show the spectrum of the density of states, which corresponds to QO of thermodynamic observables like the de Haas-van Alphen (dHvA) effect. In contrast to the SdH effect, the slow difference frequency is absent in the dHvA effect. The reason is that the latter only depends on the scattering via the Dingle factor whereas scattering dominates transport [29,33], which is also confirmed by the strong (weak) dependence of the QO signals for the top (bottom) panels. Thus, a careful comparison between QO frequencies of SdH and dHvA can confirm our unusual QO without a FS orbit.

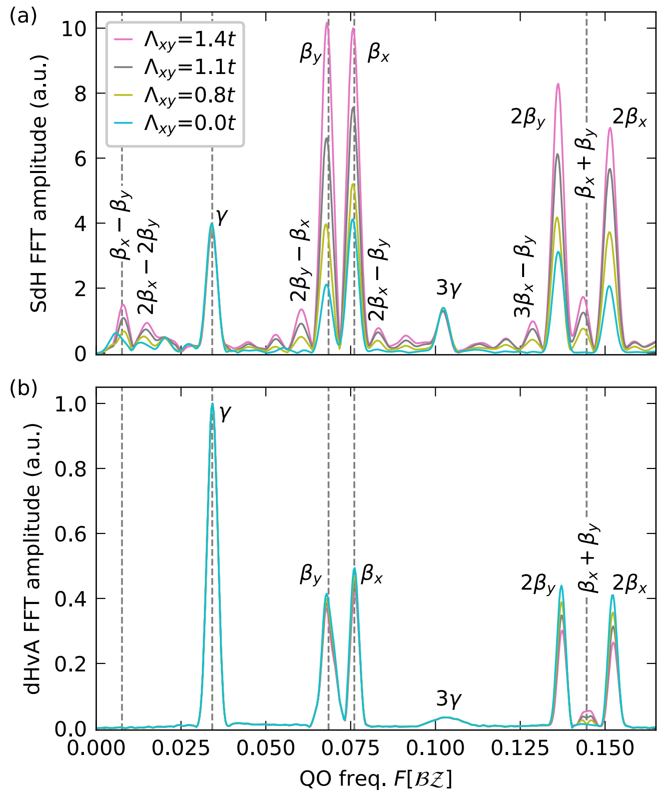

FIG. 3. Numerically computed QO spectra for the parameters regime generating the FSs shown in Fig. 2(a). In (a) we analyzed the conductance whereas in (b) we analyzed the density of states $\rho(\mu)$. The theoretical prediction for the three basis frequencies and the sum and difference frequency, based on the area of the FSs, are indicated as gray dashed lines.

Discussion and conclusion. We have shown that a robust slow QO frequency emerges in minimal models of iron chalcogenides. The key ingredients were the broken rotational symmetry between the electron pockets in the nematic phase and an efficient coupling between these pockets. The latter can originate from an orbital selective scattering, e.g., a dominating impurity contribution of the d_{xy} orbital. We provided full numerical lattice calculations with orbital magnetic fields, which also confirm recent analytical works on difference frequency QOs without semiclassical orbits beyond the Onsager relation [29,33]. However, the weak main peak splitting in Fig. 1(d) of the degnerate frequencies for sizable impurity scattering point towards nonperturbative effects. Further supporting evidence of our scenario is that the experimentally extracted masses from the temperature dependence of the QOs [11] is in accordance with our analytical predictions [33], namely the mass of the slow frequency roughly equals the difference of the ones of the electron pockets.

Of course, neither our effective two-band nor the three-orbital model (which is already challenging numerically) captures all details of the complicated electronic structure of iron chalcogenides [37]. In fact, we have neglected any correlation effects, which could further increase scattering between the electron pockets, e.g., by collective spin fluctuations. However, our scenario requires no preconditions except a finite coupling of the electron pockets via scattering. Therefore, we expect our scenario to be reproducible in any microscopic model of iron chalcogenides. In summary, we argue that our results are a robust feature of the nematic phase of iron chalcogenides and elucidate that no additional pocket of a nematic Lifshitz transition is required to explain the QO experiments [11,12].

The correct assignment of QO frequencies with putative FS orbits is crucial for correctly identifying the electronic structure in iron chalcogenides and beyond. Alas, our scenario of sharp QOs without FS orbits further complicates the interpretation of QO data. However, it also provides novel insights into subtle details of quasiparticle scattering otherwise inaccessible in experiments. Furthermore, the quotient of the difference frequency and mass in the vicinity of the nematic phase transition is directly related to the order parameter $(\beta_x - \beta_y)(\lambda)/(m_{\beta_x} + m_{\beta_y})(\lambda) \propto \delta\mu(\lambda) \propto (\lambda_c - \lambda)^\alpha$, see SM [47], and therefore provides direct access to the critical exponent α. A precise measurement can reveal the nature of the nematic quantum phase transition by determining deviations to the mean-field behavior of $\alpha = 1/2$.

We showed that the slow QO frequency of iron chalcogenides can be explained by the presence of orbital selective impurity scattering, which has implications for the SC pairing symmetry. It is normally expected that impurities, as necessarily present in heavily disordered $FeSe_{1-x}S_x$ [51], suppress $s^\pm$ superconductivity [52,53]. However, the orbital selective scattering does not couple the electron and hole pockets, which would be detrimental for $s^\pm$ pairing. Thus, the new QO mechanism possibly explains the robustness of superconductivity in the iron chalcogenides. We hope that the observation and quantification of similar QO frequencies can lead to a more precise identification of the electronic structure of other correlated electron materials.

Note added. The emergence of a slow frequency together with peak splitting occurs also in other platforms. Unexplained experimental data for gate voltage-dependent Rashba spin splitting in GaAs [54], in which magneto-inter-sub-band oscillations were discovered, show similar behavior.

Code and data related to this paper are available on Zenodo [55] from the authors upon reasonable request.

Acknowledgments. We acknowledge helpful discussion and related collaborations with N. Huber, M. Wilde and C. Pfleiderer. We thank A. Chubukov, A. Coldea, and T. Shibauchi, for helpful discussions and comments on the manuscript. V.L. acknowledges support from the Studienstiftung des deutschen Volkes. J.K. acknowledges support from the Imperial-TUM flagship partnership. We acknowledge support from the Munich Quantum Valley, which is supported by the Bavarian state government with funds from the Hightech Agenda Bayern Plus and the Deutsche Forschungsgemeinschaft (DFG, German Research Foundation) TRR 360 – 492547816.

[1] A. Damascelli, Z. Hussain, and Z.-X. Shen, Angle-resolved photoemission studies of the cuprate superconductors, Rev. Mod. Phys. **75**, 473 (2003).

[2] D. H. Lu, M. Yi, S.-K. Mo, A. S. Erickson, J. Analytis, J.-H. Chu, D. J. Singh, Z. Hussain, T. H. Geballe, I. R. Fisher *et al.*, Electronic structure of the iron-based superconductor LaOFeP, Nature (London) **455**, 81 (2008).

[3] P. Richard, T. Qian, and H. Ding, ARPES measurements of the superconducting gap of Fe-based superconductors and their implications to the pairing mechanism, J. Phys.: Condens. Matter **27**, 293203 (2015).

[4] M. Yi, Y. Zhang, Z.-X. Shen, and D. Lu, Role of the orbital degree of freedom in iron-based superconductors, npj Quantum Mater. **2**, 57 (2017).

[5] D. Shoenberg, *Magnetic Oscillations in Metals* (Cambridge University Press, Cambridge, 1984).

[6] N. Doiron-Leyraud, C. Proust, D. LeBoeuf, J. Levallois, J.-B. Bonnemaison, R. Liang, D. A. Bonn, W. N. Hardy, and L. Taillefer, Quantum oscillations and the Fermi surface in an underdoped high-T_c superconductor, Nature (London) **447**, 565 (2007).

[7] S. E. Sebastian, N. Harrison, and G. G. Lonzarich, Towards resolution of the Fermi surface in underdoped high-T_c superconductors, Rep. Prog. Phys. **75**, 102501 (2012).

[8] S. E. Sebastian, J. Gillett, N. Harrison, P. H. C. Lau, D. J. Singh, C. H. Mielke, and G. G. Lonzarich, Quantum oscillations in the parent magnetic phase of an iron arsenide high temperature superconductor, J. Phys.: Condens. Matter **20**, 422203 (2008).

[9] T. Terashima, N. Kurita, M. Tomita, K. Kihou, C.-H. Lee, Y. Tomioka, T. Ito, A. Iyo, H. Eisaki, T. Liang *et al.*, Complete Fermi surface in $BaFe_2As_2$ observed via Shubnikov–de Haas oscillation measurements on detwinned single crystals, Phys. Rev. Lett. **107**, 176402 (2011).

[10] A. I. Coldea, D. Braithwaite, and A. Carrington, Iron-based superconductors in high magnetic fields, C. R. Phys. **14**, 94 (2013).

[11] A. I. Coldea, S. F. Blake, S. Kasahara, A. A. Haghighirad, M. D. Watson, W. Knafo, E. S. Choi, A. McCollam, P. Reiss, T. Yamashita, M. Bruma, S. C. Speller, Y. Matsuda, T. Wolf, T. Shibauchi, and A. J. Schofield, Evolution of the low-temperature Fermi surface of superconducting $FeSe_{1-x}S_x$ across a nematic phase transition, npj Quantum Mater. **4**, 2 (2019).

[12] P. Reiss, D. Graf, A. A. Haghighirad, W. Knafo, L. Drigo, M. Bristow, A. J. Schofield, and A. I. Coldea, Quenched nematic criticality and two superconducting domes in an iron-based superconductor, Nat. Phys. **16**, 89 (2020).

[13] L. Onsager, Interpretation of the de Haas-van Alphen effect, Philos. Mag. J. Sci. **43**, 1006 (1952).

[14] B. S. Tan, Y.-T. Hsu, B. Zeng, M. C. Hatnean, N. Harrison, Z. Zhu, M. Hartstein, M. Kiourlappou, A. Srivastava, M. D. Johannes *et al.*, Unconventional Fermi surface in an insulating state, Science **349**, 287 (2015).

[15] P. Czajka, T. Gao, M. Hirschberger, P. Lampen-Kelley, A. Banerjee, J. Yan, D. G. Mandrus, S. E. Nagler, and N. P. Ong, Oscillations of the thermal conductivity in the spin-liquid state of α-$RuCl_3$, Nat. Phys. **17**, 915 (2021).
[16] J. Knolle and N. R. Cooper, Quantum oscillations without a Fermi surface and the anomalous de Haas–van Alphen effect, Phys. Rev. Lett. **115**, 146401 (2015).
[17] L. Zhang, X.-Y. Song, and F. Wang, Quantum oscillation in narrow-gap topological insulators, Phys. Rev. Lett. **116**, 046404 (2016).
[18] J. Knolle and N. R. Cooper, Excitons in topological Kondo insulators: Theory of thermodynamic and transport anomalies in SmB_6, Phys. Rev. Lett. **118**, 096604 (2017).
[19] I. Sodemann, D. Chowdhury, and T. Senthil, Quantum oscillations in insulators with neutral Fermi surfaces, Phys. Rev. B **97**, 045152 (2018).
[20] O. Erten, P. Ghaemi, and P. Coleman, Kondo breakdown and quantum oscillations in SmB_6, Phys. Rev. Lett. **116**, 046403 (2016).
[21] D. Chowdhury, Y. Werman, E. Berg, and T. Senthil, Translationally invariant non-Fermi-liquid metals with critical Fermi surfaces: Solvable models, Phys. Rev. X **8**, 031024 (2018).
[22] H. Shen and L. Fu, Quantum oscillation from in-gap states and a non-Hermitian Landau level problem, Phys. Rev. Lett. **121**, 026403 (2018).
[23] P. A. Lee, Quantum oscillations in the activated conductivity in excitonic insulators: Possible application to monolayer WTe_2, Phys. Rev. B **103**, L041101 (2021).
[24] V. Leeb, K. Polyudov, S. Mashhadi, S. Biswas, R. Valentí, M. Burghard, and J. Knolle, Anomalous quantum oscillations in a heterostructure of graphene on a proximate quantum spin liquid, Phys. Rev. Lett. **126**, 097201 (2021).
[25] A. A. Allocca and N. R. Cooper, Low-frequency quantum oscillations from interactions in layered metals, Phys. Rev. Res. **3**, L042009 (2021).
[26] A. A. Allocca and N. R. Cooper, Quantum oscillations in interaction-driven insulators, SciPost Phys. **12**, 123 (2022).
[27] A. A. Allocca and N. R. Cooper, Fluctuation-dominated quantum oscillations in excitonic insulators, arXiv:2302.06633.
[28] V. Leeb and J. Knolle, Quantum oscillations in a doped Mott insulator beyond Onsager's relation, Phys. Rev. B **108**, 085106 (2023).
[29] N. Huber, V. Leeb, A. Bauer, G. Benka, J. Knolle, C. Pfleiderer, and M. A. Wilde, Quantum oscillations of the quasiparticle lifetime in a metal, Nature (London) **621**, 276 (2023).
[30] V. Polyanovsky, Magnetointersubband oscillations of conductivity in a two-dimensional electronic system, Fiz. Tekh. Poluprovodn. **22**, 1408 (1988).
[31] M. E. Raikh and T. V. Shahbazyan, Magnetointersubband oscillations of conductivity in a two-dimensional electronic system, Phys. Rev. B **49**, 5531 (1994).
[32] N. S. Averkiev, L. E. Golub, S. A. Tarasenko, and M. Willander, Theory of magneto-oscillation effects in quasi-two-dimensional semiconductor structures, J. Phys.: Condens. Matter **13**, 2517 (2001).
[33] V. Leeb and J. Knolle, Theory of difference-frequency quantum oscillations, Phys. Rev. B **108**, 054202 (2023).
[34] M. D. Watson, T. Yamashita, S. Kasahara, W. Knafo, M. Nardone, J. Béard, F. Hardy, A. McCollam, A. Narayanan, S. F. Blake, T. Wolf, A. A. Haghighirad, C. Meingast, A. J. Schofield, H. v. Löhneysen, Y. Matsuda, A. I. Coldea, T. Shibauchi, Dichotomy between the hole and electron behavior in multiband superconductor FeSe probed by ultrahigh magnetic fields, Phys. Rev. Lett. **115**, 027006 (2015).
[35] S. Kasahara, T. Watashige, T. Hanaguri, Y. Kohsaka, T. Yamashita, Y. Shimoyama, Y. Mizukami, R. Endo, H. Ikeda, K. Aoyama *et al.*, Field-induced superconducting phase of FeSe in the BCS-BEC cross-over, Proc. Natl. Acad. Sci. USA **111**, 16309 (2014).
[36] T. Terashima, N. Kikugawa, A. Kiswandhi, E.-S. Choi, J. S. Brooks, S. Kasahara, T. Watashige, H. Ikeda, T. Shibauchi, Y. Matsuda, T. Wolf, A. E. Böhmer, F. Hardy, C. Meingast, H. v. Löhneysen, M.-T. Suzuki, R. Arita, and S. Uji, Anomalous Fermi surface in FeSe seen by Shubnikov–de Haas oscillation measurements, Phys. Rev. B **90**, 144517 (2014).
[37] A. I. Coldea and M. D. Watson, The key ingredients of the electronic structure of FeSe, Annu. Rev. Condens. Matter Phys. **9**, 125 (2018).
[38] S.-H. Baek, D. V. Efremov, J. M. Ok, J. S. Kim, J. van den Brink, and B. Büchner, Orbital-driven nematicity in FeSe, Nat. Mater. **14**, 210 (2015).
[39] T. Shimojima, Y. Suzuki, T. Sonobe, A. Nakamura, M. Sakano, J. Omachi, K. Yoshioka, M. Kuwata-Gonokami, K. Ono, H. Kumigashira *et al.*, Lifting of xz/yz orbital degeneracy at the structural transition in detwinned FeSe, Phys. Rev. B **90**, 121111(R) (2014).
[40] C. A. Occhialini, J. J. Sanchez, Q. Song, G. Fabbris, Y. Choi, J.-W. Kim, P. J. Ryan, and R. Comin, Spontaneous orbital polarization in the nematic phase of FeSe, Nat. Mater. **22**, 985 (2023).
[41] A. I. Coldea, Electronic nematic states tuned by isoelectronic substitution in bulk $FeSe_{1-x}S_x$, Front. Phys. **8**, 594500 (2021).
[42] L. Ortenzi, E. Cappelluti, L. Benfatto, and L. Pietronero, Fermi-surface shrinking and interband coupling in iron-based pnictides, Phys. Rev. Lett. **103**, 046404 (2009).
[43] M. Breitkreiz, P. M. R. Brydon, and C. Timm, Transport anomalies due to anisotropic interband scattering, Phys. Rev. B **88**, 085103 (2013).
[44] A. E. Koshelev, Magnetotransport of multiple-band nearly antiferromagnetic metals due to hot-spot scattering, Phys. Rev. B **94**, 125154 (2016).
[45] M. Daghofer, A. Nicholson, A. Moreo, and E. Dagotto, Three orbital model for the iron-based superconductors, Phys. Rev. B **81**, 014511 (2010).
[46] C. W. Groth, M. Wimmer, A. R. Akhmerov, and X. Waintal, Kwant: A software package for quantum transport, New J. Phys. **16**, 063065 (2014).
[47] See Supplemental Material at http://link.aps.org/supplemental/10.1103/PhysRevB.109.L081109. for the Hamiltonian of the three-orbital model and the quantum oscillation analysis..
[48] A. Weiße, G. Wellein, A. Alvermann, and H. Fehske, The kernel polynomial method, Rev. Mod. Phys. **78**, 275 (2006).
[49] S. Margadonna, Y. Takabayashi, M. T. McDonald, K. Kasperkiewicz, Y. Mizuguchi, Y. Takano, A. N. Fitch, E. Suard, and K. Prassides, Crystal structure of the new $FeSe_{1-x}$ superconductor, Chem. Commun., 5607 (2008).
[50] H. Bruus and K. Flensberg, *Many-Body Quantum Theory in Condensed Matter Physics: An Introduction*, Oxford Graduate Texts (Oxford University Press, Oxford, 2004).

[51] S. Teknowijoyo, K. Cho, M. A. Tanatar, J. Gonzales, A. E. Böhmer, O. Cavani, V. Mishra, P. J. Hirschfeld, S. L. Bud'ko, P. C. Canfield *et al.*, Enhancement of superconducting transition temperature by pointlike disorder and anisotropic energy gap in FeSe single crystals, Phys. Rev. B **94**, 064521 (2016).

[52] D. V. Efremov, M. M. Korshunov, O. V. Dolgov, A. A. Golubov, and P. J. Hirschfeld, Disorder-induced transition between $s_{\pm}$and s_{++} states in two-band superconductors, Phys. Rev. B **84**, 180512(R) (2011).

[53] A. Chubukov, Pairing mechanism in Fe-based superconductors, Annu. Rev. Condens. Matter Phys. **3**, 57 (2012).

[54] M. J. Rendell, S. D. Liles, A. Srinivasan, O. Klochan, I. Farrer, D. A. Ritchie, and A. R. Hamilton, Gate voltage dependent Rashba spin splitting in hole transverse magnetic focusing, Phys. Rev. B **105**, 245305 (2022).

[55] V. Leeb and J. Knolle, Interband scattering- and nematicity-induced quantum oscillation frequency in FeSe, https://zenodo.org/doi/10.5281/zenodo.8225406.